Nanodevices

DOI: 10.1002/smll.200600271

In Situ Electron Microscopy Electromechanical Characterization of a Bistable NEMS Device

*Changhong Ke and Horacio D. Espinosa**

A previously proposed two-terminal carbon-nanotube-based device with closed-loop feedback is demonstrated through in situ scanning electron microscopy (SEM) experiments. The pull-in/pull-out tests were carried out using a multi-walled carbon nanotube (MWCNT) welded to a conductive probe attached to a nanomanipulator. The MWCNTs were cantilevered over a gold electrode and electrostatically actuated. The measured current–voltage curves exhibited the theoretically predicted hysteretic loop between the pull-in and pull-out processes. Both experiments and theoretical modeling demonstrated the bistability of the device confirming its utility in applications such as memory elements, NEMS switches, and logic devices. Failure mechanisms observed during the pull-in/pull-out event are also reported and discussed.

Keywords:
- bistability
- carbon nanotubes
- memory elements
- nanoelectromechanical systems (NEMS)
- tunneling

1. Introduction

Carbon nanotubes (CNTs) are a type of one-dimensional material structure with unique electrical, mechanical, and chemical properties. Based on the understanding achieved during the past decade, in relation to their electromechanical properties, manipulation, and growth, these nanostructures are considered ideal building blocks for nanoelectromechanical systems (NEMS). Some prototype carbon-nanotube-based NEMS devices have recently been proven functional, such as nonvolatile random access memory elements,[1] nanotweezers,[2,3] tunable oscillators,[4] nanorelays,[5–7] and nanoswitches.[8,9]

A two-terminal nanotube-based cantilever device with feedback control was also recently proposed;[10] such a device is schematically shown in Figure 1. The device consists of a conductive nanotube mounted on a top electrode as a freestanding cantilever above a bottom electrode. When a bias voltage is applied between the nanotube cantilever and the bottom electrode, through a circuit containing a resistor R, the nanotube deflects towards the bottom electrode under the electrostatic force. Equilibrium is achieved as long as the elastic force from the deflection of the nanotube cantilever balances the electrostatic force acting on the nanotube. However, when the applied voltage exceeds the so-called "pull-in voltage", the nanotube loses its stability and deflects abruptly towards the bottom electrode. When the gap between the cantilever tip and bottom electrode is below ≈1 nm, a tunneling current flows through the circuit. Due to this current and the presence of the resistor R in the circuit, the voltage drop across the nanotube tip and the bottom electrode decreases, leading to a new equilibrium position. After stabilization, a decrease in applied voltage results in a current reduction in the circuit. When the volt-

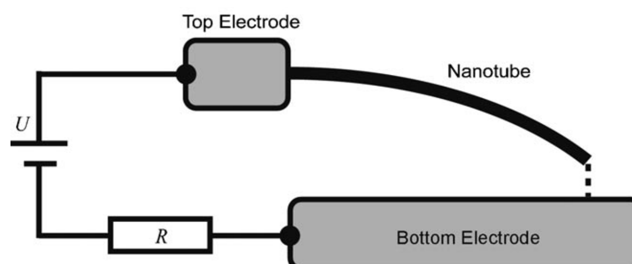

Figure 1. Schematic of a two-terminal nanotube device with feedback control through the incorporation of the resistor R in the circuit.

[*] C. Ke, H. D. Espinosa
Department of Mechanical Engineering
Northwestern University, Evanston, IL 60208-3111 (USA)
Fax: (+1) 847-491-3915
E-mail: espinosa@northwestern.edu

© 2006 Wiley-VCH Verlag GmbH & Co. KGaA, Weinheim

age drops to a certain value, called the “pull-out voltage”, the nanotube cantilever is released from the position in contact with the bottom electrode. Thus, the device exhibits two well-defined stable equilibrium positions and a hysteretic loop[5,9] in the current–voltage space between the pull-in and pull-out processes. Applications that can exploit such device behavior include NEMS switches, random-access memory elements, and logic devices. In this paper, we experimentally demonstrate this unique electromechanical behavior by means of in situ scanning electron microscopy (SEM) testing. We also present failure modes observed during the pull-in/pull-out processes.

2. Results and Discussion

2.1. In Situ SEM Experiments

The in situ SEM testing configuration employed in the study is schematically shown in Figure 2. The multi-walled carbon nanotubes (MWCNTs) used in the experiments were synthesized by chemical vapor deposition[11] (First Nano, Inc., Ronkonkoma, NY). Transmission electron microscopy (TEM) images of the nanotubes confirmed their concentric graphene layered structures. The diameter of the nanotubes exhibited a distribution in the range of 10–130 nm and their length varied in the range of 1–20 μm. By employing a three-axes nanomanipulator possessing 1-nm positioning accuracy (Klocke Nanotechnik, Germany), a single carbon nanotube was welded to the tip of a tungsten manipulator probe inside a scanning electron microscopy (LEO 1525) chamber.[12] The welding was performed by electron-beam-induced deposition (EBID) of Pt or hydrocarbons.[3,13] The probe and MWCNT cantilever were placed parallel to an electrode consisting of a Si chip, which was coated with a Au thin film, and attached to a teflon block (Figure 2). The Si chip was vertically attached to the side of a teflon block and the ensemble mounted on an SEM sample holder. The position of the teflon block with the electrode was carefully adjusted so that only the edge could be viewed in the SEM image. A Keithley 4200 SCS semiconductor characterization system, with two medium-power source measurement units (SMUs) and two remote preamplifiers, was connected to the device by means of an electrical feed-through mounted on a port of the SEM chamber.

The system described above was used for the acquisition of current–voltage (I–U) curves. A resistor ($R=0.98$ GΩ) was employed in the measurements. The manipulator probe with the mounted nanotube cantilever was controlled to approach the electrode until a desired distance (typically 0.5–2 μm, depending on the length and the diameter of the nanotubes) was reached (see Figure 2). One such experiment, presented in Figure 3, provides the SEM images of a nanotube cantilever before voltage was applied, in the pulled-in position, and after pull-out, respectively (Figure 3 a–c). The measured I–U characteristic curve during these events is plotted in Figure 4. In this example, an MWCNT with an outer diameter of 100 nm and a length of 9 μm was placed at an angle of 40° with respect to the electrode surface. A gap of 0.9 μm between the free end of the nanotube and the gold electrode was set (see Figure 3 a). A voltage sweep from 0 V to

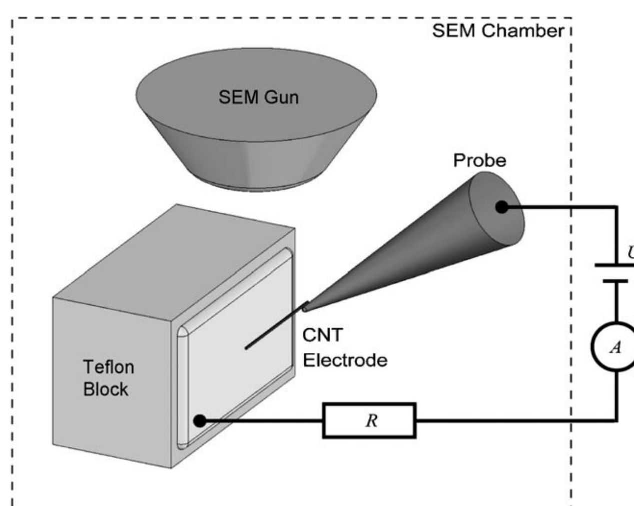

Figure 2. Schematics of the setup for in situ SEM testing of nanotube cantilever devices.

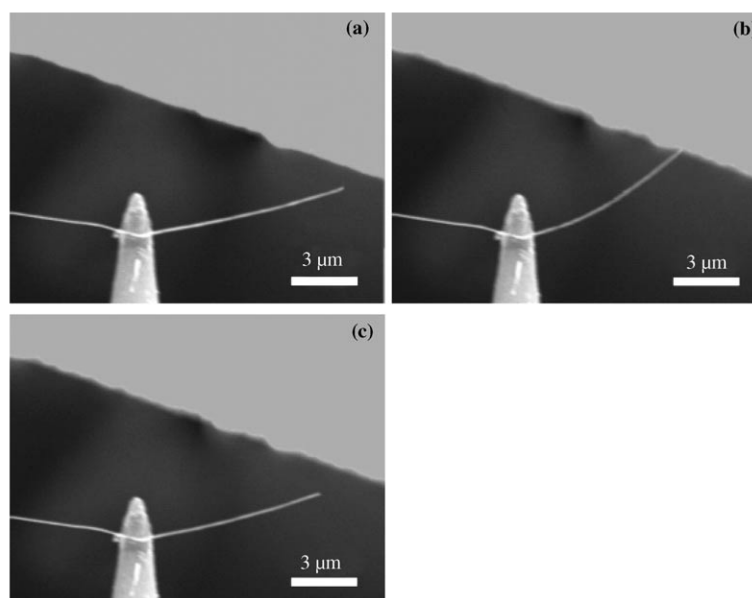

Figure 3. SEM images showing the configurations of a nanotube cantilever at different applied voltages: a) Starting configuration (applied voltage $U=0$); b) pulled-in configuration ($U=30$ V); c) cantilever configuration after pull-out ($U=1$ V).

© 2006 Wiley-VCH Verlag GmbH & Co. KGaA, Weinheim

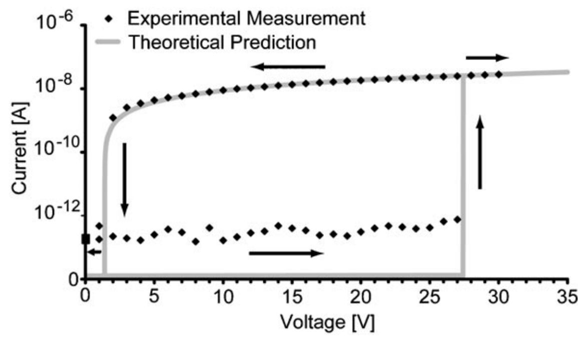

Figure 4. Comparison between experimentally measured and theoretical I–U curves. The pull-in/pull-out processes correlate with the current jumps. The arrows show the direction in which the hysteretic loop is followed during the increase and decrease of the driving voltage U.

30 V and back to 0 V at rate of 1 V s^{-1} was applied between the nanotube and the gold electrode from the Keithley instrument. Simultaneously, both the applied voltage and the current were recorded. At the lower applied voltage, the measured current was on the order of 0.1 pA, which is the noise in the circuit, likely the result of current leakage. With an increase of the applied voltage, the pull-in event occurred when U reached 28 V. Correspondingly, as shown in the I–U plot, there was a significant current jump in the circuit, from 0.1 pA to about 26 nA. The applied voltage U continued to increase to 30 V and then decreased back to 0 V. Figure 3b shows the nanotube cantilever at the pull-in position when U was kept at 30 V. The pull-out event occurred when U decreased back to 1 V. Figure 3c shows the nanotube cantilever configuration after pull-out. During the pull-out event, the measured current in the circuit jumped from 1.2 nA down to the noise level. The measured I–U curve clearly shows a hysteretic loop consistent with the theoretical prediction.

2.2. Modeling

The experimental results presented in Section 2.1. were interpreted by means of the electromechanical analysis described in Ref. [10]. The model assumes that the nanotube is a uniform linear elastic beam and a perfect conductor, and it takes into account the concentrated charge at the free end of the cantilever in the evaluation of the electrostatic and van der Waals distributed forces.[14,15] Since the in situ SEM testing configuration shown in Figure 3 had the MWCNT forming an angle α with the substrate, we performed the electromechanical analysis for the configuration schematically shown in Figure 5 in which the angle α is given by $\alpha = \sin^{-1}\left(\frac{H_2 - H_1}{L}\right)$. If the deformation of the nanotube cantilever along its axial direction is neglected, the governing equation of the deflection $w(x)$ of the nanotube cantilever is given by[15]

$$EI\frac{\mathrm{d}^4 w}{\mathrm{d}x^4} = q_{\mathrm{elec}} + q_{\mathrm{vdw}} \tag{1}$$

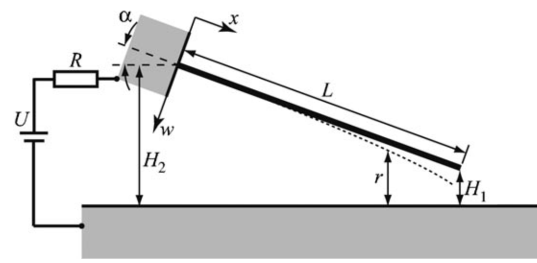

Figure 5. Schematic of the in situ SEM testing configuration corresponding to the case shown in Figure 3.

where E is the Young's modulus of the nanotube, I is the moment of inertia of the cross section (for nanotubes, $I = \frac{\pi}{64}\left(D_{\mathrm{ext}}^4 - D_{\mathrm{int}}^4\right)$, where D_{ext} and D_{int} are the outer and inner diameters of the nanotube, respectively), w is the deflection of the nanotube cantilever. The quantity q_{vdw} is the van der Waals force per unit length, which can be evaluated using the approach reported in Ref. [16], while q_{elec} is the electrostatic force per unit length acting on the nanotube, which can be approximated by the following equation based on the capacitance model given in Ref. [15]:

$$q_{\mathrm{elec}} \approx \frac{-\pi\varepsilon_0 V^2}{\sqrt{r(r+D_{\mathrm{ext}})}\,a\cosh^2\left(1+\frac{2r}{D_{\mathrm{ext}}}\right)} \frac{1+f_{\mathrm{c}}}{\cos^2\left(\alpha + \tan^{-1}\left(\frac{\mathrm{d}w}{\mathrm{d}x}\right)\right)} \tag{2}$$

In the above equation, r is the gap between the nanotube and the electrode, ε_0 ($8.854\times10^{-12}\,\mathrm{C^2N^{-1}m^{-2}}$) is the permittivity of free space, and f_{c} accounts for the concentrated charge at the free end of the nanotube cantilever, and is given by $f_c = 0.85\left[\left(H_2 + \frac{D_{\mathrm{ext}}}{2}\right)^2 \frac{D_{\mathrm{ext}}}{2}\right]^{\frac{1}{3}} \delta\left(x - x_{\mathrm{tip}}\right)$. $\delta(x)$ is the Dirac distribution function and V is the voltage drop across the gap between the free end of the nanotube and the electrode. Before the nanotube contacts the electrode, $V = U$; when the nanotube is in contact with the electrode, V can be obtained from an equivalent circuit including the tip tunneling resistance and the resistance R of the external resistor, namely:

$$\frac{V}{U}\frac{R}{R_0}\exp\left(-r\left(x_{tip}\right)/\lambda\right) = 1 - \frac{V}{U} \tag{3}$$

where U is the voltage applied from the power supply as shown in Figure 5, R_0 is the contact resistance between the nanotube and the electrode, which is usually a few hundred ohms,[17] and λ is a material constant defined by $\lambda^{-1} = 1.02\sqrt{\Phi(\mathrm{eV})}\,\mathrm{\mathring{A}}^{-1}$, with Φ being the work function (for MWCNTs and gold $\Phi \approx 5.0$ eV[18]). By solving Equations (1) and (3) simultaneously, using a numerical integration method, the I–U characteristics of the device were obtained.

2.3. Comparison between Theoretical Predictions and Experiments

A comparison between the experimental measurements and the theoretical prediction is shown in Figure 4. The pa-

© 2006 Wiley-VCH Verlag GmbH & Co. KGaA, Weinheim

rameters used in the simulation include a contact resistance $R_0=500\ \Omega$, the length of the tested nanotube $L=9\ \mu m$, and a Young's modulus $E=1$ TPa. The distances between the two ends of the nanotube and gold electrode were obtained from the SEM images as $H_1=0.9\ \mu m$ and $H_2=6.7\ \mu m$. The external diameter of the nanotube, $D_{ext}=100$ nm, was obtained from a high-magnification SEM image. Assuming that the wall of the nanotube contains 100 graphite layers (consistent with our TEM characterization) and an interlayer distance of 0.335 nm, the interior diameter of the nanotube is estimated as $D_{int}=33.67$ nm (the number of nanotube wall layers is chosen such that the theoretical prediction of the pull-in voltage, 27.8 V, matches the experimental result, 28 V). Examination of Figure 4 reveals a good agreement between experimental measurement and theoretical prediction, except for the region where the applied voltage U decreased back to 5 V and lower. In this region, the deviation between the experimental measurement and theoretical prediction increases with the decrease of the applied voltage and becomes substantial at the moment of pull-out. This deviation implies that the exponential relation between the resistance of the gap and the gap size employed in the simulation, based simply on tunneling, may not be accurate enough. The possible reasons include an increase of contact resistance due to surface contamination (likely to happen with hydrocarbons during the imaging process), and the formation of metal–insulator–metal (MIM) junctions at the point of contact. All these features may change the current–voltage characteristic of the contact region. Likewise, the energy released between the nanotube tip and impacted gold surface is another poorly understood phenomenon, which has been observed systematically in tip-to-surface discharges recorded in conductive scanning probe microscopy studies.[19] Further study, in particular, atomistic or multiscale modeling of the electrical and mechanical contact between the nanotube and the electrode should be pursued to gain insight into these issues.

2.4. Device Failure Modes

The in situ SEM experiments also revealed device failure modes. One such failure consisted in the lost of tube material at the free end after each pull-in/pull-out cycle. In one such experiment, the length of the tube was measured to drop from 9 to 7.9 μm after one pull-in/pull-out cycle, and from 7.9 to 7.2 μm after another cycle. The shortening of the nanotube translated to the steady increase of the pull-in voltage even when the tip–substrate gap was adjusted to be constant. This phenomenon was consistently observed during several repeated pull-in/pull-out experiments on devices with similar geometries, that is, similar tube length, diameter, and gap with the substrate. Through careful digital-image processing of the SEM images of the nanotube at different stages (before test, pull-in, and pull-out), we identified that the shortening of the nanotube happened during the pull-in processes. Although similar phenomena have been mentioned in the literature,[3,8] the mechanism is still not well understood. It is believed that such device failure is related to the dynamical behavior of the pull-in process. Although failure modes of carbon nanotubes, such as mechanical fracture[20–22] and electrical breakdown,[23,24] have been investigated intensively, most of the reported results are in the quasi-static or steady-state regimes and only concerned with a single effect, that is, either mechanical or electrical response. Failure modes of nanotube-based NEMS, in the context of actual working conditions, remain vastly unexplored.

To gain insight into the observed failure, we performed a dynamics analysis to examine the transient response of the device during the pull-in event. While the detailed modeling of the pull-in dynamics will be presented elsewhere,[25] the relevant findings are reported here. The analysis revealed that in devices with a geometry similar to the one shown in Figure 3, the speed of the tube free end at the moment of contacting the electrode can be as high as $200\ m\,s^{-1}$. Because of the finite deformation of the nanotube cantilever, its impact with the electrode generates a strong elastic compression wave propagating along the nanotube. Through the dynamic analysis of the device, it was estimated that a compressive stress as high as 30 GPa was generated. This compression stress is superimposed to a bending stress of about an order of magnitude smaller with a maximum-stress location along the cantilever as a function of time. One can then conclude that if there is any significant defect on the body of the nanotube, which is likely unavoidable for MWCNTs, the nanotube would break at some distance from the impacting end, similar to the breaking of dynamically compressed brittle rods.[26,27] The remains of the nanotube cantilever can then settle in a pull-in position corresponding to a shorter tube if the electrostatic and van der Waals forces are larger than the elastic-restitution force.

The above hypothesis was confirmed by a separate in situ SEM pull-in experiment, as shown in Figure 6. The experimental configuration shown in Figure 2 was employed, except for the orientation of the electrode surface, which was carefully adjusted such that features on the electrode surface could be visualized at grazing incidence with the electron beam. Figure 6a shows a nanotube (from the same batch of nanotubes as the one employed in the pull-in/pull-out test shown in Figure 3) mounted on to a manipulator probe, which was placed parallel to the electrode surface. The length and the diameter of the nanotube were measured to be 6 μm and 80 nm, respectively. The pull-in event happened when the applied voltage reached 19.2 V. Figure 6b shows the position of the nanotube cantilever after pull-in had occurred. It can be clearly seen that part of the nanotube at the free end was broken and remained attached to the electrode surface. The remaining part of the tube was still in contact with the electrode. Therefore, stress-wave-induced fracture appears to be a plausible explanation for the aforementioned shortening of the nanotube.

From the above discussion of failure mechanisms, it is envisioned that failure of nanotube devices can be minimized or even avoided if the device geometry (cantilever length, diameter, and gap) is optimized and high-quality and defect-free nanotubes are used. Development of reliable

© 2006 Wiley-VCH Verlag GmbH & Co. KGaA, Weinheim

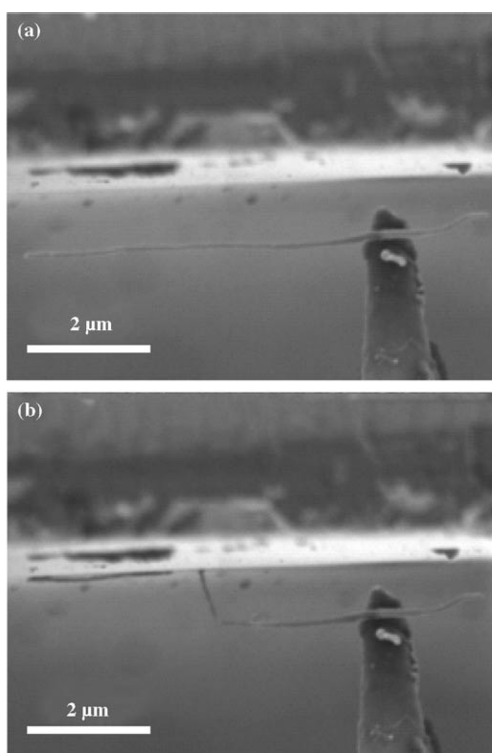

Figure 6. SEM images corresponding to an experiment in which the nanotube cantilever fractured. The device is shown before (a) and after (b) the pull-in process.

computational tools to design and optimize such nanodevices is an area that needs further investigation. Although the task is quite challenging, these are imperative steps to manufacture carbon-nanotube-based functional devices with adequate reliability.

3. Conclusions

In this paper, the functioning of a two-terminal nanotube-based nanodevice with a closed-loop feedback control mechanism was experimentally demonstrated by in situ SEM testing. An electromechanical analysis was employed to interpret the experimental current–voltage measurements. Both experimental and theoretical modeling demonstrated the bistability of the device, which can be employed advantageously in applications such as memory elements, NEMS switches, and logic devices. Shortening of the nanotube cantilever was observed in the experiments during the pull-in process. Stress-wave-induced CNT fracture as a result of mechanical impact during the pull-in event was proposed to account for such device failure, which was supported by a separate in situ SEM experiment. The failure mechanism shows that in order to design reliable NEMS devices, it is imperative to gain a fundamental understanding of failure modes as a function of configuration parameters. Ultimately, maps defining regions of robust device operation need to be developed. Importantly, the in situ SEM testing methodology reported in this paper is generic, and as such it can be advantageously employed to investigate other types of nanotube- or nanowire-based nanoelectromechanical devices.

Acknowledgements

The authors acknowledge the support of the FAA through Award No. DTFA03-01-C-00031 and the NSF through award No. CMS-0120866. We would like to express our appreciation to Drs. J. Newcomb and J. Larsen-Base for supporting this work. Work was also supported in part by the Nanoscale Science and Engineering Initiative of the National Science Foundation under NSF Award No. EEC-0118025. We also thank Dr. N. Moldovan and Dr. Y. Zhu for assistance with the nanomanipulation and in situ SEM testing.

[1] T. Rueckes, K. Kim, E. Joselevich, G. Y. Tseng, C. L. Cheung, C. M. Lieber, *Science* **2000**, *289*, 94 – 97.
[2] P. Kim, C. M. Lieber, *Science* **1999**, *286*, 2148 – 2150.
[3] S. Akita, Y. Nakayama, S. Mizooka, Y. Takano, T. Okawa, Y. Miyatake, S. Yamanaka, M. Tsuji, T. Nosaka, *Appl. Phys. Lett.* **2001**, *79*, 1691 – 1693.
[4] V. Sazonova, Y. Yaish, H. Ustunel, D. Roundy, T. A. Arias, P. L. McEuen, *Nature* **2004**, *431*, 284 – 287.
[5] J. M. Kinaret, T. Nord, S. Viefers, *Appl. Phys. Lett.* **2003**, *82*, 1287 – 1289.
[6] L. M. Jonsson, T. Nord, J. M. Kinaret, S. Viefers, *J. Appl. Phys.* **2004**, *96*, 629 – 635.
[7] S. W. Lee, D. S. Lee, R. E. Morjan, S. H. Jhang, M. Sveningsson, O. A. Nerushev, Y. W. Park, E. E. B. Campbell, *Nano Lett.* **2004**, *4*, 2027 – 2030.
[8] J. E. Jang, S. N. Cha, Y. Choi, G. A. J. Amaratunga, D. J. Kang, D. G. Hasko, J. E. Jung, J. M. Kim, *Appl. Phys. Lett.* **2005**, *87*, 163114.
[9] E. Dujardin, V. Derycke, M. F. Goffman, R. Lefevre, J. P. Bourgoin, *Appl. Phys. Lett.* **2005**, *87*, 193107.
[10] C. H. Ke, H. D. Espinosa, *Appl. Phys. Lett.* **2004**, *85*, 681 – 683.
[11] W. Z. Li, S. S. Xie, L. X. Qian, B. H. Chang, B. S. Zou, W. Y. Zhou, R. A. Zhao, G. Wang, *Science* **1996**, *274*, 1701 – 1703.
[12] C. H. Ke, N. Pugno, B. Peng, H. D. Espinosa, *J. Mech. Phys. Solids* **2005**, *53*, 1314 – 1333.
[13] M. F. Yu, O. Lourie, M. J. Dyer, K. Moloni, T. F. Kelly, R. S. Ruoff, *Science* **2000**, *287*, 637 – 640.
[14] C. H. Ke, H. D. Espinosa, *J. Appl. Mech.* **2005**, *72*, 721 – 725.
[15] C. H. Ke, H. D. Espinosa, N. Pugno, *J. Appl. Mech.* **2005**, *72*, 726 – 731.
[16] M. Dequesnes, S. V. Rotkin, N. R. Aluru, *Nanotechnology* **2002**, *13*, 120 – 131.
[17] R. Tarkiainen, M. Ahlskog, J. Penttila, L. Roschier, P. Hakonen, M. Paalanen, E. Sonin, *Phys. Rev. B* **2001**, *64*, 195412.
[18] R. P. Gao, Z. W. Pan, Z. L. Wang, *Appl. Phys. Lett.* **2001**, *78*, 1757 – 1759.
[19] D. F. Farson, H. W. Choi, S. I. Rokhlin, *Nanotechnology* **2006**, *17*, 132 – 139.
[20] T. Belytschko, S. P. Xiao, *Int. J. Multiscale Comp. Engr.* **2003**, *1*, 115 – 126.
[21] D. Troya, S. L. Mielke, G. C. Schatz, *Chem. Phys. Lett.* **2003**, *382*, 133 – 141.
[22] O. Lourie, H. D. Wagner, *Appl. Phys. Lett.* **1998**, *73*, 3527 – 3529.
[23] J. Y. Huang, S. Chen, S. H. Jo, Z. Wang, D. X. Han, G. Chen, M. S. Dresselhaus, Z. F. Ren, *Phys. Rev. Lett.* **2005**, *94*, 236802.

 © 2006 Wiley-VCH Verlag GmbH & Co. KGaA, Weinheim

small NANO MICRO

[24] T. D. Yuzvinsky, W. Mickelson, S. Aloni, S. L. Konsek, A. M. Fennimore, G. E. Begtrup, A. Kis, B. C. Regan, A. Zettl, *Appl. Phys. Lett.* **2005**, *87*, 083 103.
[25] C. H. Ke, N. Moldovan, H. D. Espinsoa, unpublished results.
[26] B. Audoly, S. Neukirch, *Phys. Rev. Lett.* **2005**, *95*, 095 505.
[27] J. R. Gladden, N. Z. Handzy, A. Belmonte, E. Villermaux, *Phys. Rev. Lett.* **2005**, *94*, 035 503.

Received: June 2, 2006
Published online on October 6, 2006

 © 2006 Wiley-VCH Verlag GmbH & Co. KGaA, Weinheim